molecules

MDPI

Article

Dual-Enzyme Cascade Composed of Chitosan Coated FeS_2 Nanozyme and Glucose Oxidase for Sensitive Glucose Detection

Bowen Shen [1], Molan Qing [2], Liying Zhu [2], Yuxian Wang [3] and Ling Jiang [1,3,*]

[1] State Key Laboratory of Materials-Oriented Chemical Engineering, College of Biotechnology and Pharmaceutical Engineering, Nanjing 211816, China
[2] School of Chemistry and Molecular Engineering, Nanjing Tech University, Nanjing 210009, China
[3] College of Food Science and Light Industry, Nanjing Tech University, Nanjing 210009, China
* Correspondence: jiangling@njtech.edu.cn

Abstract: Immobilizing enzymes with nanozymes to catalyze cascade reactions overcomes many of the shortcomings of biological enzymes in industrial manufacturing. In the study, glucose oxidases were covalently bound to FeS_2 nanozymes as immobilization carriers while chitosan encapsulation increased the activity and stability of the immobilized enzymes. The immobilized enzymes exhibited a 10% greater increase in catalytic efficiency than the free enzymes while also being more stable and catalytically active in environments with an alkaline pH of 9.0 and a high temperature of 100 °C. Additionally, the FeS_2 nanozyme-driven double-enzyme cascade reaction showed high glucose selectivity, even in the presence of lactose, dopamine, and uric acid, with a limit of detection (LOD) (S/N = 3) as low as 1.9×10^{-6} M. This research demonstrates that nanozymes may be employed as ideal carriers for biological enzymes and that the nanozymes can catalyze cascade reactions together with natural enzymes, offering new insights into interactions between natural and synthetic biosystems.

Keywords: nanozyme; immobilized enzyme; double-enzyme cascade; glucose detection

Citation: Shen, B.; Qing, M.; Zhu, L.; Wang, Y.; Jiang, L. Dual-Enzyme Cascade Composed of Chitosan Coated FeS_2 Nanozyme and Glucose Oxidase for Sensitive Glucose Detection. *Molecules* **2023**, *28*, 1357. https://doi.org/10.3390/molecules28031357

Academic Editor: Gordon Morris

Received: 27 December 2022
Revised: 18 January 2023
Accepted: 26 January 2023
Published: 31 January 2023

1. Introduction

As with mostly protein-based biological catalysts, enzymes accelerate chemical reactions by reducing activation energy [1]. Due to their great substrate specificity and high catalytic efficiency, natural enzymes have significant uses in biochemical analysis, medicine, chemical synthesis, and food preparation [2–5]. However, the usage of enzymes is costly, their recycling is challenging, and their tertiary protein structure is easily damaged under harsh process conditions, resulting in the loss of catalytic activity [6–8]. Additionally, the stability of enzymes must meet strict standards in the industrial manufacturing environment, greatly restricting the broader industrial application of enzymes to date [9–11].

Accordingly, enhancing enzyme stability in harsh environments is a good strategy to promote the use of enzymes [12,13]. Enzyme immobilization by encasing them in solid substances or restricting them to certain regions using physical or chemical methods enables their reuse while also greatly increasing their stability and catalytic efficiency [14–17]. Additionally, the immobilization of enzymes makes it easier to separate enzymes from products, culture medium, and substrates, which improves process economics [18,19]. Conventional enzyme-immobilization carriers are chemically inert and have no catalytic effect themselves [14,20,21]. Some carrier materials even limit the contact between the substrate and the enzyme, thereby affecting the catalytic efficiency. Additionally, certain carriers will interact with the enzyme to reduce its ability to catalyze reactions [22–24]. Therefore, the most important factor for successful enzyme immobilization is the selection of an appropriate carrier material [25].

The creation of new and highly effective nanozymes is another strategy for addressing the shortcomings of enzymes [26,27]. Since in 2007 it was discovered that Fe_3O_4 has enzyme-like capabilities, nanozymes have gained significant attention [28]. Nanozymes

are frequently employed in medicine and sensing because of their benefits for the easy combination of active sites, high stability, and simple synthesis [29–31]. Although it has been noted that nanozymes can imitate the activities of oxidases, peroxidases, and hydrolases, little is known about how nanozymes interact with other enzymes [26]. As an upgraded version of the typical Fe_3O_4 nanozyme, iron sulfide (FeS_2) nanozymes have excellent enzyme-like catalytic activity, mimic the properties of other enzymes, and have abundant active sites such as amino and sulfhydryl groups [32,33]. Moreover, many active groups of FeS_2 are ideal conjugation sites for enzyme immobilization, while their defect-prone structures and active surface groups promote non-covalent interactions with natural enzymes [34,35]. The scope of catalytic reactions can theoretically be greatly expanded by combining enzymatic processes and nanozymes, enabling the implementation of advanced cascade reactions. Chemical reactions are also facilitated by electron transport on the nanozyme surface [36,37].

In our previous research, iron ions and cysteine were used to create FeS_2 nanozymes, which showed good peroxidase-like activity [38]. Due to its durability, chemical inertness, and flexibility, chitosan is an ideal polysaccharide material that may be employed as a carrier for enzyme reactions. We constructed an immobilized enzyme system based on chitosan (CS) encapsulation and covalent binding of nanozymes, demonstrating a high glucose oxidase (Gox) loading capacity and enhanced Gox stability in harsh environments. Notably, the presence of nanozymes enhanced the catalytic activity and stability of Gox. In addition, biological enzymes and nanozymes can support cascade reactions that catalyze the production of hydroxyl radicals from glucose, making it possible to detect glucose in urine.

2. Results and Discussion

2.1. Characterization of FeS_2/CS@Gox

In order to assess the state of the immobilized enzyme, the morphology of the FeS_2 enzyme particles was first studied. The FeS_2 nanomaterial exhibited a homogeneous hexagonal nanosheet shape (Figure S1), whereas the FeS_2 with immobilized enzymes had a hexagonal nanosheet shape with compound surface attachments (Figure 1A). When Gox was loaded onto the surface of FeS_2 nanosheets, polymeric attachments were clearly visible (Figure 1B). The enzyme is physically and chemically bonded to the surface of FeS_2, preserving the FeS_2's original form in the composite material. The establishment of the link between FeS_2 and Gox was then confirmed by FTIR (Figure 1C and Figure S2), and the typical absorption peak of cysteine-rich FeS_2 nanosheets was observed at 3300–3400 cm^{-1} which was attributed to the NH stretching vibration. The symmetric and asymmetric stretching vibrations of CH and CH_2 were reflected in the peaks at 2750 and 3200 cm^{-1} [39]. The presence of S-H groups in FeS_2 was confirmed by the weak signal at 2550 cm^{-1}. Stretching vibrations of the C=O molecule resulted in both asymmetric and symmetric peaks at 1600–1700 cm^{-1}. The broad peak at 900–1300 cm^{-1} was attributed to C=S double bonds, while the broad peak at 1600–1700 cm^{-1} can be attributed to the newly formed C=O of NH_2 in FeS_2 and COOH in Gox after conjugation with CS and Gox. The N-H bending vibration caused a peak at 1538 cm^{-1}, while the vibration peaks at 1295 and 1059 were related to the C-O and C-N stretching vibrations, respectively. The distinctive infrared functional group peaks demonstrate the chemical interaction between FeS_2 and Gox. The successful conjugation was further confirmed by the elemental distribution in Fe/CS@Gox (Figure S3). Finally, pure FeS_2 displayed distinct crystal characteristic peaks, which also demonstrated that FeS_2 had been successfully prepared. The same crystal characteristic peaks also developed in FeS_2 when the enzyme was immobilized. The consistency of the XRD pattern also demonstrated that Gox and CS did not alter the structure of FeS_2 after immobilization (Figure 1D). FeS_2 can efficiently exhibit its catalytic activity provided that its crystal structure remains unaffected, which is advantageous for the creation of immobilized enzyme systems. These results confirmed that Gox was successfully grafted onto the FeS_2 nanosheets.

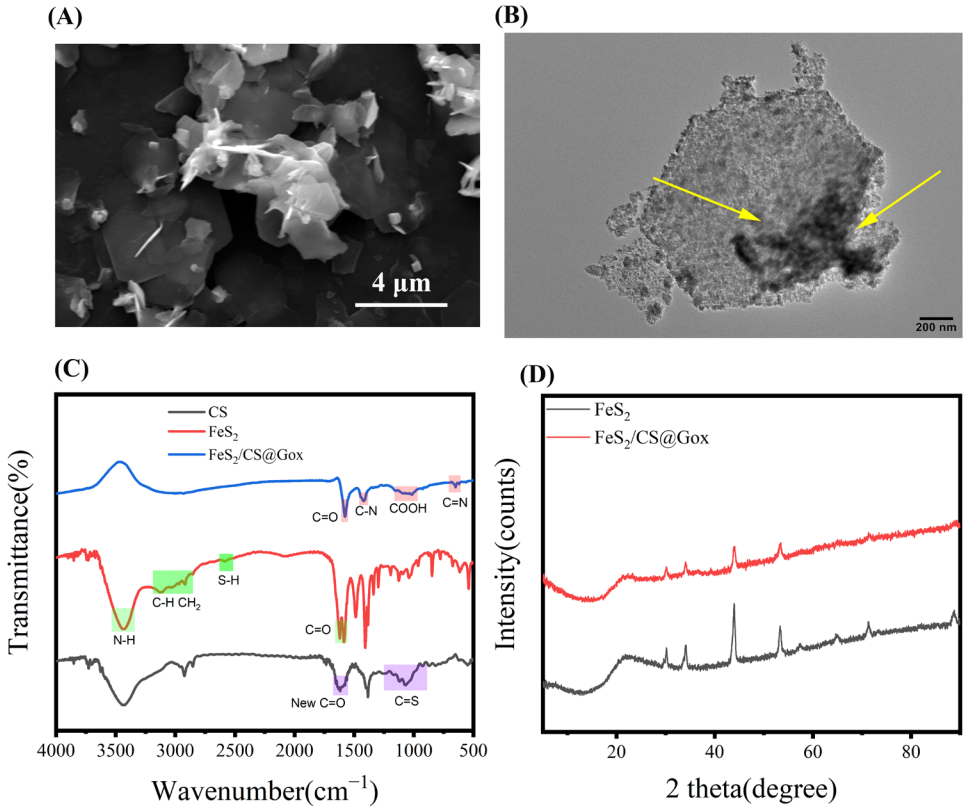

Figure 1. (**A**) The SEM picture of FeS_2/CS@Gox. (**B**) The TEM picture of FeS_2/CS@Gox (The yellow arrow points to the attachment on FeS_2). (**C**) The FTIR of CS, FeS_2 and FeS_2/CS@Gox. (**D**) The XRD pattern of FeS_2 and FeS_2/CS@Gox.

2.2. Immobilization Ratio and Immobilized Enzyme Activity

The conjugation of Gox to the FeS_2 nanosheets was confirmed by green fluorescent labeling. As shown in Figure S4, there was a clearly visible green fluorescence under ultraviolet light which confirmed the presence of Gox in the FeS_2/CS particles. Furthermore, fluorescence microscopy of the FeS_2/CS@Gox particles showed that FeS_2 exhibited an aggregated morphology in the field of view, and bright green fluorescence coincided with the distribution of FeS_2 (Figure 2A,B). Subsequently, we investigated the effect of adding different amounts of Gox to the enzyme immobilization ratio. The enzyme immobilization did not exceed 30% when only FeS_2 and Gox were linked covalently, but the FeS_2/CS had higher immobilization efficiency. FeS_2/CS had the highest efficiency and loading capacity when Gox was added at 0.5 mg, which was the most suitable concentration for enzyme immobilization in this system (Table S1 and Figure 2C). In an aqueous solution, Gox readily self-dissociates when it is directly chemically bound to FeS_2, but CS creates a confined space for FeS_2@Gox, making Gox dissociation challenging. The effects of pH and temperature on immobilized enzymes were then further investigated. As shown in Figure 2D,E, the immobilized enzyme exhibited higher catalytic activity than the free enzyme, which may be due to the attachment to the support changing the functional groups of the enzyme. In addition, it has been reported that the sulfide helps to enhance the activity of the enzyme, and the catalytic activity of Gox can be significantly improved by the numerous thiol groups in FeS_2 [40]. Additionally, the immobilized enzymes demonstrated improved catalytic activity in extreme circumstances. The immobilized enzyme may retain more than 80% of its catalytic activity in acidic and alkaline environments, whereas the catalytic activity of the free enzyme is less than 60%. The catalytic activity of enzymes is also impacted by temperature. Free enzymes barely exhibit any catalytic activity at 100 °C, but immobilized enzymes exhibit more than 60% catalytic activity. The results demonstrated that the stability and catalytic activity of the enzyme were significantly improved by immobilizing it with

FeS_2 and CS. Reusability is a crucial aspect of immobilized enzymes, and Figure 2F shows the reuse of the FeS_2/CS@Gox. The catalytic efficiency of FeS_2/CS@Gox remained above 80% over the first eight reuse cycles, but further usage eventually resulted in structural degradation and a loss of mass transfer, which would lower catalytic performance [41]. The use of enzyme engineering in actual manufacturing will be encouraged by its excellent reusability, which will lower costs and boost yield.

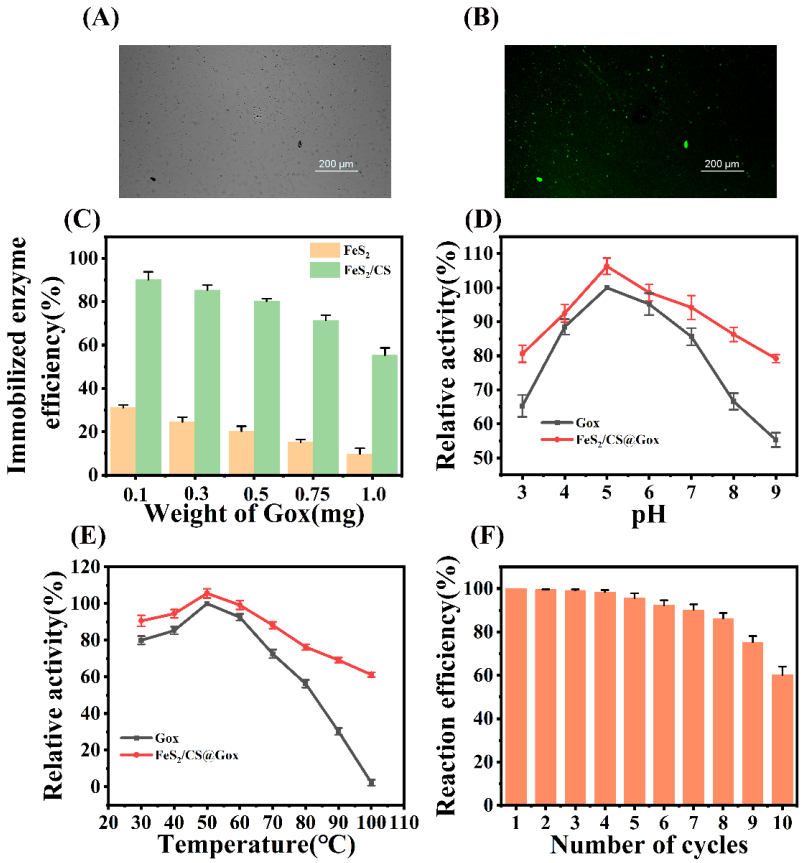

Figure 2. (**A**) Image of the immobilized enzyme under a confocal laser microscope. (**B**) Green fluorescence of the immobilized enzyme. (**C**) Immobilized enzyme efficiency of FeS_2 and FeS_2/CS (**D**) Effect of pH on Catalytic Efficiency of Immobilized Enzymes. (**E**) The Effect of Temperature on the Catalytic Efficiency of Immobilized Enzymes. (**F**) Reuse Efficiency of Immobilized Enzymes.

2.3. The POD-like Activity of FeS_2

Subsequently, we investigated the peroxidase-like catalytic capacity of the composite through the oxidation of 3,3′,5,5′-tetramethylbenzidine (TMB) in the presence of H_2O_2. We tested the effects of nFeS concentration, H_2O_2 concentration, pH, and temperature on the peroxidase-like activity. With the increase of FeS_2 concentration, the oxidation rate of TMB also increased (Figure 3B). Moreover, with the increase of H_2O_2 concentration, the rate of TMB oxidation also gradually increased (Figure 3C). After optimizing the temperature and pH for the peroxidase-like activity of nFeS, it was found that the peroxidase-like activity of FeS_2 decreased with the increase in temperature, and the optimum pH was 4.0 (Figure 3D,E). The above results show that the peroxidase-like catalytic performance of FeS_2 nanoparticles is dependent on catalyst concentration, substrate concentration, temperature, and pH, similar to natural enzymes. The mechanism of peroxidase-like activity of FeS_2 nanoparticles was then further explored. Terephthalic acid was used as a fluorescent probe to detect the production of hydroxyl radicals, which can be produced from H_2O_2 by peroxidase [42]. The generation of hydroxyl radicals from H_2O_2 catalyzed by FeS_2 was detected. In the presence of H_2O_2, FeS_2 can convert TA into TA-OH, which has increased fluorescence intensity. The production of hydroxyl radicals was detected under acidic

or neutral conditions, indicating that the peroxidase-like activity of FeS_2 is due to its ability to decompose H_2O_2 to produce hydroxyl radicals (Figure S5). To determine the catalytic efficiency of FeS_2 nanosheets, we performed enzyme kinetic analysis with testing at optimal pH and room temperature. Unexpectedly, FeS_2 nanosheets showed a very high affinity for H_2O_2, with a K_m of 0.01743 mM and a V_{max} of 110.9848 nM/s (Figure 3F). The results demonstrate that FeS_2 mimics natural peroxidase catalytically and has the benefit of stability over natural enzymes. The excellent peroxidase-like activity of FeS_2 nanosheets encouraged us to further apply them for two-enzyme coupled catalysis.

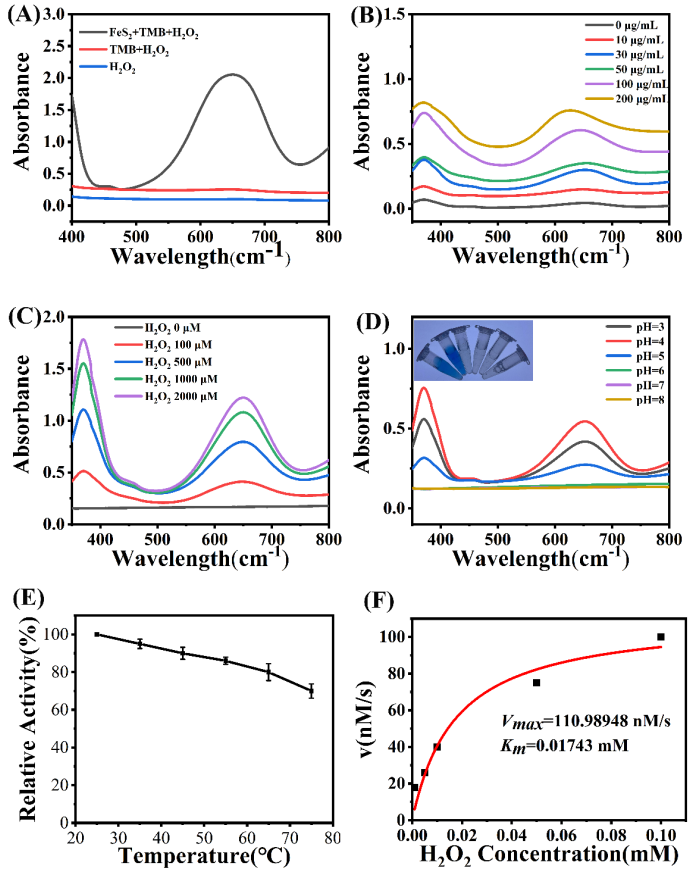

Figure 3. (**A**) UV−vis absorbance spectra changes of TMB in different reaction systems. (**B**) UV−vis absorbance spectra changes of TMB in different concentrations of FeS_2. (**C**,**D**) UV−vis absorbance spectra changes of TMB in different concentrations of H_2O_2. (**E**) The effect of temperature on the catalytic activity of POD-like FeS_2. (**F**) Kinetic assay for the POD-like activity of FeS_2 nanozymes with H_2O_2 as substrate.

2.4. Sensitivity and Selectivity of Glucose Detection

Based on the exceptional peroxidase-mimicking activity of FeS_2, we initially employed the immobilized Gox-TMB system to detect glucose in a solution. With the increase of glucose content, the absorbance at 652 nm of the detecting system also increased (Figure 4A). The color response of the immobilized Gox-TMB system showed a good linear relationship with the glucose concentration (Figure 4B). Moreover, the detection limit was as low as 1.9×10^{-6} M, which was sufficiently sensitive for the actual glucose sample. We created a standard color card with the colors representing the various glucose concentrations in order to more easily determine the concentration of glucose in the solution (Figure 4C). The selectivity was assessed by examining the reactions to the typical interfering substances, including the selectivity of FeS_2 for H_2O_2 and the selectivity of the system for glucose. At the same substrate concentration, only H_2O_2 produced the response of FeS_2, while there was no reaction with common metal ions and TMB, demonstrating its strong selectivity for H_2O_2 (Figure S6). Similarly, only glucose caused a discernible change in solution color, while the

solutions containing interfering compounds remained colorless and behaved exactly like the blank, clearly demonstrating the great selectivity for glucose (Figure 4D and Figure S7). The FeS_2/CS@Gox system's strong selectivity and sensitivity for glucose make it suited for the identification of samples that contain the substance. In addition, the catalytic efficiency of the glucose detection system based on FeS_2/CS@Gox was further evaluated over time. As shown in Figure 4E, the catalytic activity of the glucose detection system decreased during one month of storage, but the overall value was higher than 80%, demonstrating the good storage stability of the glucose detection system. The good shelf life of the FeS_2/CS@Gox system will also further improve its application in the detection of real samples. The nanozyme-based glucose-sensing system offers a good detection limit [43], and our system offers obvious benefits over other systems (Table 1). In conclusion, the FeS_2/CS@Gox system constructed by the immobilized enzyme strategy has excellent sensitivity, selectivity, and shelf life and is a potential product for glucose detection.

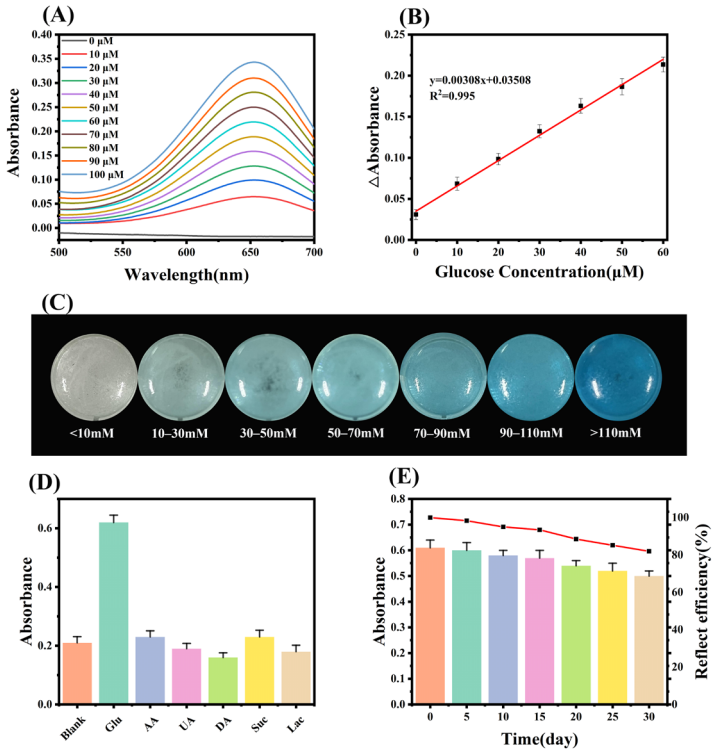

Figure 4. (**A**) UV–vis absorption spectra of FeS_2/CS@Gox in different glucose concentrations. (**B**) Linear calibration curve of the absorbance at 652 nm against glucose concentration. (**C**) Standard color chart of glucose concentration and color change of FeS_2/CS@Gox. (**D**) Selectivity toward glucose of the above system against potential interfering substances. (**E**) Shelf life of the glucose detection system.

Table 1. Comparison of the colorimetric glucose sensors using various artificial peroxidase.

Material	Bioassay Type	Linear Range	LOD(μM)	Ref.
FeS_2	Solution	0–60 μM	1.9 μM	This work
Fe SSN	Solution	0–60 μM	2.1 μM	[44]
Fe_3O_4	Solution	62.5–500 μM	50 μM	[45]
CoO-OMC	Solution	0–500 mM	68 μM	[46]
Au-Ag-Pt	Solution	0–10 mM	289.6 μM	[47]

2.5. Glucose Detection in Actual Samples

Patients suffering from kidney disease or diabetes have high levels of glucose in their urine, and their physical condition can be judged by detecting the glucose content in urine or blood [48,49]. To assess the viability of FeS_2/CS@Gox, we created a mixed solution that

contained glucose to mimic actual samples. The standard color card provides a rough estimate of the concentration of glucose when the test sample reacts with the detection system (Figure 5A). The glucose concentration in the sample to be tested was further judged by measuring the absorbance, and the glucose concentration that was calculated using the standard curve is shown in Table 2 and Figure 5B. When we compared the detected concentration to the actual concentration of the material to be tested, there was only a slight discrepancy, and the error was less than 3%. This finding demonstrates that the glucose detection system based on FeS_2/CS@Gox can determine the concentration of glucose present in different complex samples, such as blood and urine. In addition, we can also detect glucose in blood and sweat using the FeS_2/CS@Gox system, and the stability based on the FeS_2/CS@Gox system can be applied to the development and production of glucose detection medical devices.

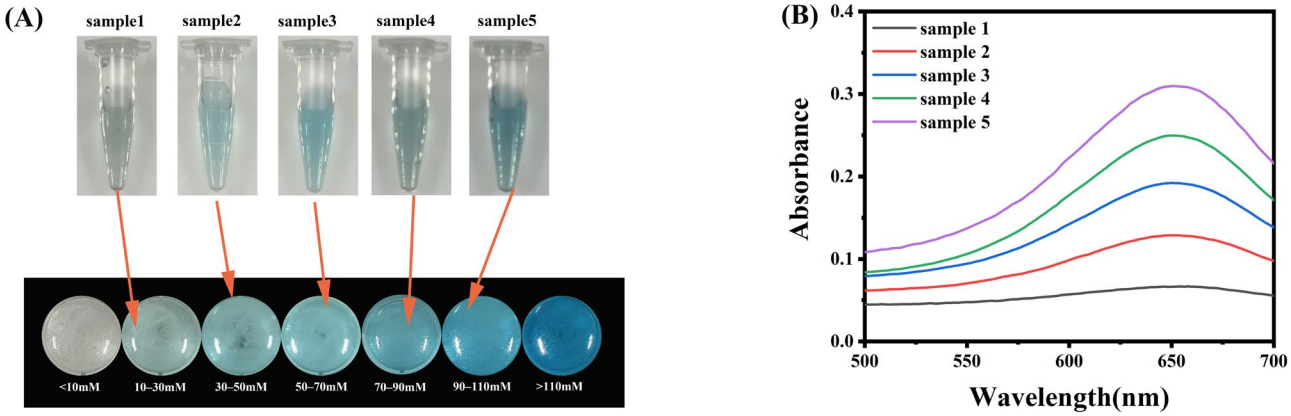

Figure 5. (**A**) Actual detection of color changes for different samples. (**B**) UV–vis absorbance spectra changes for different samples.

Table 2. The actual detection effect of different samples.

Sample	Abs	Con (μM)	Actual Con (μM)	Error (%)
Sample 1	0.06669	10.263	10	2.63
Sample 2	0.12885	30.445	30	1.48
Sample 3	0.19211	50.984	50	1.97
Sample 4	0.24967	69.672	70	0.05
Sample 5	0.30984	89.208	90	0.88

3. Materials and Methods

3.1. Materials

The reagents were purchased from commercial sources and were used without further purification. Ferric chloride ($FeCl_3$) was purchased from Macklin (Shanghai, China). Cysteine and 3,3′,5,5′-tetramethylbenzidine (TMB) were purchased from Sigma-Aldrich (Shanghai, China). Chitosan (CS) and Glucose oxidase (Gox) were purchased from Sangon Biotech (Shanghai, China). DNS Reducing Sugar Detection Kits were purchased from Solarbio (Beijing, China).

3.2. Synthesis and Characterization of FeS_2

FeS_2 was synthesized as described previously, with minor modifications as follow [38]. Briefly, 0.5 g of $FeCl_3$ and 1.0 g of cysteine were dissolved in 40 mL of ethylene glycol, and then 3.6 g sodium acetate was added. The mixture was then allowed to react for 12 h at 200 °C in an autoclave. The produced black powder was collected, washed with ethanol three times, and dried at 60 °C.

3.3. Immobilization of Gox

In order to promote covalent conjugation, Gox and FeS_2 were mixed in 0.1 mM phosphate buffer with pH = 9 and reacted at 37 °C for 24 h under constant stirring at 12,000 rpm. The solids were then separated, added to the CS solution without washing, and left for 10 min to allow chitosan to coat the alkaline FeS_2 surface. FeS_2 particles containing Gox and CS were centrifuged, washed three times with distilled water, and lyophilized. The loading of the FeS_2 particles with the enzyme was confirmed by the FITC fluorescent labeling and confocal laser scanning microscopy (Nikon, Tokyo, Japan) [50].

3.4. Materials Characterization

The morphology of the prepared FeS_2 and FeS_2/CS@Gox was observed using a scanning electron microscope (SEM, S4800). The solid sample was dispersed in absolute ethanol, dried on a silicon wafer, scanned, and photographed using SEM. A transmission electron microscope (TEM) was used to further analyze the morphology of FeS_2/CS@Gox. FeS_2/CS@Gox was dispersed in an ethanol solution, dried on a copper grid, and then examined and photographed under the TEM. The dried product was positioned on a quartz glass slide for X-ray diffraction examination (XRD) (Rigaku Miniflex 600, Tokyo, Japan). With 0.008 θ steps and a 3-degree-per-minute scanning speed, the scanning range was 5 to 60 degrees. In order to prepare the FeS_2 and FeS_2/CS@Gox powders for Fourier transform infrared spectroscopy, they were combined with dry KBr powder in an agate mortar, crushed to a fine powder, and then heated to remove any leftover moisture. After being formed into a pellet, the combined powder was scanned using the device. For the Fourier transform infrared spectrum of the Gox solution, KBr was first made into thin slices, and then a small amount of Gox solution was dropped on the KBr thin slices and scanned by the instrument.

3.5. The Effect of pH on the Activity of Immobilized Enzyme

To study the effect of pH on free enzymes and immobilized enzymes, the free enzymes and immobilized enzymes were put in different pH reaction systems to catalyze glucose, the enzyme activities under different conditions were recorded, and the highest activity of the free enzymes was defined as 100% relative enzyme activity.

3.6. The Effect of Temperature on the Activity of Immobilized Enzyme

To study the effect of temperature on free enzymes and immobilized enzymes, the free enzymes and immobilized enzymes were put in different temperature reaction systems to catalyze glucose, the enzyme activities under different conditions were recorded, and the highest activity of the free enzymes was defined as 100% relative enzyme activity.

3.7. POD-Like Activity and Kinetic Assay of FeS_2 Nanozyme

TMB was used as the substrate for the measurement of peroxidase-like (POD-like) activity with H_2O_2. Different concentrations of H_2O_2 and FeS_2 were mixed in a phosphate buffer with pH = 4.5, and 10 μL of 80 mM TMB solution was then added. The absorbance of the mixture at 652 nm was assessed using a UV-vis spectrophotometer (Perkin Elmer, Waltham, MA, USA) after 5 min of reaction at 37 °C [42].

The nanozyme's affinity for its substrate was assessed by measuring the Michaelis constant (K_M) defined as the substrate concentration at which the nanozyme exhibits half the maximum reaction rate. Maximum reaction velocity (V_{max}) was defined as the maximum reaction rate measured at a saturated substrate concentration. The kinetic constants K_M and V_{max} were determined using Origin software, by fitting the substrate concentrations and initial reaction velocities (v) to the Michaelis-Menten equation:

$$v = (V_{max} \times [S])/(K_M + [S]) \quad (1)$$

where [S] is the substrate concentration. The initial reaction velocity was calculated using the equation:

$$v = \triangle A/(\triangle t \times \varepsilon \times L) \quad (2)$$

where $\triangle$A is the value of the change in absorbance before and after the reaction; $\triangle$t (s) is the reaction time; ε (M^{-1} cm^{-1}) = 39000 is the molar absorption coefficient of the colorimetric substrate, and L (cm) is the width of the quartz cuvette [32].

3.8. Enzyme Activity Assay of Gox

The reducing sugar assay was used to measure the amount of glucose consumed. Briefly, 100 μL of the Gox reaction mixture containing residual glucose was mixed with 200 μL of DNS reagent and heated at 100 °C for 10 min. Then 900 μL of distilled water was added to the mixture, and the absorbance at 540 nm was measured. The consumption of glucose was used to calculate the enzyme activity titer of Gox.

3.9. Immobilized Enzyme Cycle Assay

In short, the enzyme activity of Gox in the FeS_2/CS/Gox system was determined first, and the FeS_2/CS/Gox system was filtered and dried after the reaction was complete. For subsequent enzymatic activity assays, the FeS_2/CS/Gox system obtained above was used. Enzyme activity was recorded for each reaction.

3.10. Construction of the System for Glucose Detection

The system for glucose detection consisted of 1mg of FeS_2/CS@Gox, 890 μL of 0.1 M phosphate buffer (pH = 4.5), and 10 μL of TMB (80 mM). The amount of 100 μL of the sample to be tested was then added to the glucose detection system. After 5 min of reaction at room temperature, the absorbance at 652 nm was measured, and the glucose concentration was determined using a standard curve. The LOD was calculated using the equation:

$$LOD = 3 \cdot \sigma / s \quad (3)$$

where σ is the standard deviation of 20 measurements, and *s* is the slope of the standard curve.

3.11. The Selectivity of FeS_2 for H_2O_2 Detection and Glucose Detection

The selectivity of FeS_2 for H_2O_2 was detected in solutions containing H_2O_2 (1 mM) or disrupters (1 mM). These assays were tested in the solution which contained TMB (1 mM) and FeS_2 (100 μg mL^{-1}). Color change of the above solutions was observed at 2 min, and their absorbance was recorded at 652 nm. Pure HAc-NaAc buffer was used as a control.

The selectivity of the FeS_2/CS/Gox system for glucose was detected in a solution containing glucose (50 μM) or disrupters (50 μM). The amount of 100 μL of glucose solution (100 μM) or other interfering chemicals (100 μM) was mixed with 100 μL of 1 mg mL^{-1} FeS_2/CS/Gox system. Finally, a color change of the above solutions was observed, and their absorbance was recorded at 652 nm.

3.12. Preparation of Urine Simulant

For the preparation of the urine-simulated solution, a certain amount of glucose was dissolved in water first, and then the same amount of amino acids and urea as the glucose was added. After thorough mixing, impurities were filtered out and stored at 4 °C for future use. For the urine-simulated solution, the glucose content is known, and the FeS_2/CS/Gox system is used to measure the glucose content in the solution and compare it with the actual content.

3.13. Shelf Life of the Glucose Detection System Assay

The effectively created FeS_2/CS@Gox system was dispersed in an aqueous solution initially, and then it was kept in an aqueous solution for various amounts of time to assess

its stability. Glucose was detected by the Gox system, and the stability of the FeS_2/CS@Gox system was assessed using absorbance at 652 nm.

4. Conclusions

In this study, we used FeS_2 nanozymes to encapsulate Gox, and the resulting immobilized enzyme system demonstrated increased catalytic efficiency and resistance to harsh conditions. FeS_2/CS@Gox was further used to construct a glucose detection system with great selectivity, sensitivity, and accuracy which has the potential to be applied to the actual detection of glucose in urine and blood. This system demonstrates that nanozymes may be efficient carriers of natural enzymes and that the cascade interaction between nanozymes and natural enzymes is a powerful strategy for advancing the use of natural enzymes. It is anticipated that the biocatalytic catalyst nanozyme will serve as a link between biological and abiotic catalysis.

Supplementary Materials: The following supporting information can be downloaded at: https://www.mdpi.com/article/10.3390/molecules28031357/s1. Table S1: Immobilized enzyme efficiency; Figure S1: Morphology of FeS_2; Figure S2: FTIR absorption spectrum of Gox; Figure S3: Elemental distribution of FeS_2/CS@Gox; Figure S4: The Color of FeS_2/CS@Gox under UV light; Figure S5: Hydroxyl radicals produced by FeS_2; Figure S6: Selectivity of FeS_2 to H_2O_2; Figure S7: Selectivity of FeS_2/CS@Gox to glucose.

Author Contributions: Conceptualization, B.S. and M.Q.; methodology, B.S. and L.Z.; software, B.S.; validation, B.S. and Y.W.; formal analysis, M.Q.; investigation, Y.W.; data curation, B.S.; writing—original draft preparation, B.S. and M.Q.; writing—review and editing, B.S. and L.Z.; visualization, L.Z. and L.J.; supervision, L.Z. and L.J.; project administration, L.Z. and L.J.; funding acquisition, L.J. All authors have read and agreed to the published version of the manuscript.

Funding: This work was supported by the Natural Key R&D Program of China (2021YFC2102700), the National Natural Science Foundation of China (31922070, U2106228), the Jiangsu Synergetic Innovation Center for Advanced Bio-Manufacture (XTC2205).

Institutional Review Board Statement: Not applicable.

Informed Consent Statement: Not applicable.

Data Availability Statement: Not applicable.

Conflicts of Interest: The authors declare that they have no known competing financial interests or personal relationships that could have appeared to influence the work reported in this paper.

References

1. Liu, D.-M.; Chen, J.; Shi, Y.-P. Advances on methods and easy separated support materials for enzymes immobilization. *TrAC Trends Anal. Chem.* **2018**, *102*, 332–342. [CrossRef]
2. Qiao, F.; Chen, L.; Li, X.; Li, L.; Ai, S. Peroxidase-like activity of manganese selenide nanoparticles and its analytical application for visual detection of hydrogen peroxide and glucose. *Sens. Actuators B Chem.* **2014**, *193*, 255–262. [CrossRef]
3. Nguyen, H.H.; Lee, S.H.; Lee, U.J.; Fermin, C.D.; Kim, M. Immobilized Enzymes in Biosensor Applications. *Materials* **2019**, *12*, 121. [CrossRef]
4. Metkar, S.K.; Girigoswami, K. Diagnostic biosensors in medicine—A review. *Biocatal. Agric. Biotechnol.* **2019**, *17*, 271–283. [CrossRef]
5. Wen, L.; Edmunds, G.; Gibbons, C.; Zhang, J.; Gadi, M.R.; Zhu, H.; Fang, J.; Liu, X.; Kong, Y.; Wang, P.G. Toward Automated Enzymatic Synthesis of Oligosaccharides. *Chem. Rev.* **2018**, *118*, 8151–8187. [CrossRef]
6. Hartmann, M.; Kostrov, X. Immobilization of enzymes on porous silicas–benefits and challenges. *Chem. Soc. Rev.* **2013**, *42*, 6277–6289. [CrossRef]
7. Ren, S.; Li, C.; Jiao, X.; Jia, S.; Jiang, Y.; Bilal, M.; Cui, J. Recent progress in multienzymes co-immobilization and multienzyme system applications. *Chem. Eng. J.* **2019**, *373*, 1254–1278. [CrossRef]
8. Liang, S.; Wu, X.-L.; Xiong, J.; Zong, M.-H.; Lou, W.-Y. Metal-organic frameworks as novel matrices for efficient enzyme immobilization: An update review. *Coord. Chem. Rev.* **2020**, *406*, 213194. [CrossRef]
9. Chapman, J.; Ismail, A.; Dinu, C. Industrial Applications of Enzymes: Recent Advances, Techniques, and Outlooks. *Catalysts* **2018**, *8*, 238. [CrossRef]

10. Yushkova, E.D.; Nazarova, E.A.; Matyuhina, A.V.; Noskova, A.O.; Shavronskaya, D.O.; Vinogradov, V.V.; Skvortsova, N.N.; Krivoshapkina, E.F. Application of Immobilized Enzymes in Food Industry. *J. Agric. Food Chem.* **2019**, *67*, 11553–11567. [CrossRef]
11. Xiong, W.; Liu, B.; Shen, Y.; Jing, K.; Savage, T.R. Protein engineering design from directed evolution to de novo synthesis. *Biochem. Eng. J.* **2021**, *174*, 108096. [CrossRef]
12. Basso, A.; Serban, S. Industrial applications of immobilized enzymes—A review. *Mol. Catal.* **2019**, *479*, 110607. [CrossRef]
13. Hu, Y.; Dai, L.; Liu, D.; Du, W.; Wang, Y. Progress & prospect of metal-organic frameworks (MOFs) for enzyme immobilization (enzyme/MOFs). *Renew. Sustain. Energy Rev.* **2018**, *91*, 793–801.
14. Liu, D.-M.; Dong, C. Recent advances in nano-carrier immobilized enzymes and their applications. *Process Biochem.* **2020**, *92*, 464–475. [CrossRef]
15. Reis, C.; Sousa, E.; Serpa, J.; Oliveira, R.; Oliveira, R.; Santos, J. Design of Immobilized Enzyme Biocatalysts: Drawbacks and Opportunities. *Química Nova* **2019**, *42*, 768–783. [CrossRef]
16. Ashkan, Z.; Hemmati, R.; Homaei, A.; Dinari, A.; Jamlidoost, M.; Tashakor, A. Immobilization of enzymes on nanoinorganic support materials: An update. *Int. J. Biol. Macromol.* **2021**, *168*, 708–721. [CrossRef]
17. Zhu, L.; Shen, B.; Song, Z.; Jiang, L. Permeabilized TreS-Expressing Bacillus subtilis Cells Decorated with Glucose Isomerase and a Shell of ZIF-8 as a Reusable Biocatalyst for the Coproduction of Trehalose and Fructose. *J. Agric. Food Chem.* **2020**, *68*, 4464–4472. [CrossRef]
18. Sheldon, R.A.; Basso, A.; Brady, D. New frontiers in enzyme immobilisation: Robust biocatalysts for a circular bio-based economy. *Chem. Soc. Rev.* **2021**, *50*, 5850–5862. [CrossRef]
19. Cheng, K.; Svec, F.; Lv, Y.; Tan, T. Hierarchical Micro- and Mesoporous Zn-Based Metal-Organic Frameworks Templated by Hydrogels: Their Use for Enzyme Immobilization and Catalysis of Knoevenagel Reaction. *Small* **2019**, *15*, e1902927. [CrossRef]
20. Xie, J.; Zhang, Y.; Simpson, B. Food enzymes immobilization: Novel carriers, techniques and applications. *Curr. Opin. Food Sci.* **2022**, *43*, 27–35. [CrossRef]
21. Cui, J.; Feng, Y.; Lin, T.; Tan, Z.; Zhong, C.; Jia, S. Mesoporous Metal-Organic Framework with Well-Defined Cruciate Flower-Like Morphology for Enzyme Immobilization. *ACS Appl. Mater. Interfaces* **2017**, *9*, 10587–10594. [CrossRef] [PubMed]
22. Prlainovic, N.; Bezbradica, D.; Knezevic-Jugovic, Z.; Marinkovic, A.; Mijin, D. Immobilization of enzymes onto carbon nanotubes. *Hem. Ind.* **2011**, *65*, 423–430. [CrossRef]
23. Li, J.J.; Yin, L.; Wang, Z.F.; Jing, Y.C.; Jiang, Z.L.; Ding, Y.; Wang, H.S. Enzyme-Immobilized Metal-Organic Frameworks: From Preparation to Application. *Chem. Asian J.* **2022**, *17*, e202200751. [CrossRef] [PubMed]
24. Shen, B.; Wang, B.; Zhu, L.; Jiang, L.J.N. Properties of cobalt-and nickel-doped ZIF-8 framework materials and their application in heavy-metal removal from wastewater. *Nanomaterials* **2020**, *10*, 1636. [CrossRef] [PubMed]
25. Aggarwal, S.; Chakravarty, A.; Ikram, S. A comprehensive review on incredible renewable carriers as promising platforms for enzyme immobilization & thereof strategies. *Int. J. Biol. Macromol.* **2021**, *167*, 962–986.
26. Wu, J.; Wang, X.; Wang, Q.; Lou, Z.; Li, S.; Zhu, Y.; Qin, L.; Wei, H. Nanomaterials with enzyme-like characteristics (nanozymes): Next-generation artificial enzymes (II). *Chem. Soc. Rev.* **2019**, *48*, 1004–1076. [CrossRef]
27. Wei, H.; Wang, E. Nanomaterials with enzyme-like characteristics (nanozymes): Next-generation artificial enzymes. *Chem. Soc. Rev.* **2013**, *42*, 6060–6093. [CrossRef]
28. Gao, L.; Zhuang, J.; Nie, L.; Zhang, J.; Zhang, Y.; Gu, N.; Wang, T.; Feng, J.; Yang, D.; Perrett, S.; et al. Intrinsic peroxidase-like activity of ferromagnetic nanoparticles. *Nat. Nanotechnol.* **2007**, *2*, 577–583. [CrossRef]
29. Wang, H.; Wan, K.; Shi, X. Recent Advances in Nanozyme Research. *Adv. Mater.* **2019**, *31*, e1805368. [CrossRef]
30. Wang, Q.; Wei, H.; Zhang, Z.; Wang, E.; Dong, S. Nanozyme: An emerging alternative to natural enzyme for biosensing and immunoassay. *TrAC Trends Anal. Chem.* **2018**, *105*, 218–224. [CrossRef]
31. Jiang, D.; Ni, D.; Rosenkrans, Z.T.; Huang, P.; Yan, X.; Cai, W. Nanozyme: New horizons for responsive biomedical applications. *Chem. Soc. Rev.* **2019**, *48*, 3683–3704. [CrossRef]
32. Meng, X.; Li, D.; Chen, L.; He, H.; Wang, Q.; Hong, C.; He, J.; Gao, X.; Yang, Y.; Jiang, B.; et al. High-Performance Self-Cascade Pyrite Nanozymes for Apoptosis-Ferroptosis Synergistic Tumor Therapy. *ACS Nano* **2021**, *15*, 5735–5751. [CrossRef]
33. Xi, J.; An, L.; Huang, Y.; Jiang, J.; Wang, Y.; Wei, G.; Xu, Z.; Fan, L.; Gao, L. Ultrasmall FeS_2 Nanoparticles-Decorated Carbon Spheres with Laser-Mediated Ferrous Ion Release for Antibacterial Therapy. *Small* **2021**, *17*, e2005473. [CrossRef]
34. Huang, X.; Nan, Z. Porous 2D FeS_2 nanosheets as a peroxidase mimic for rapid determination of H_2O_2. *Talanta* **2020**, *216*, 120995. [CrossRef]
35. Ding, W.; Liu, H.; Zhao, W.; Wang, J.; Zhang, L.; Yao, Y.; Yao, C.; Song, C. A Hybrid of FeS_2 Nanoparticles Encapsulated by Two-Dimensional Carbon Sheets as Excellent Nanozymes for Colorimetric Glucose Detection. *ACS Appl. Bio. Mater.* **2020**, *3*, 5905–5912. [CrossRef]
36. Li, X.; Zhu, H.; Liu, P.; Wang, M.; Pan, J.; Qiu, F.; Ni, L.; Niu, X. Realizing selective detection with nanozymes: Strategies and trends. *TrAC Trends Anal. Chem.* **2021**, *143*, 116379. [CrossRef]
37. Zhang, C.; Chen, C.; Zhao, D.; Kang, G.; Liu, F.; Yang, F.; Lu, Y.; Sun, J. Multienzyme Cascades Based on Highly Efficient Metal-Nitrogen-Carbon Nanozymes for Construction of Versatile Bioassays. *Anal. Chem.* **2022**, *94*, 3485–3493. [CrossRef]
38. Shen, B.; Li, W.; Wang, Y.; Cheng, S.; Wang, X.; Zhu, L.; Zhang, Y.; Gao, L.; Jiang, L. Rapid capture and killing of bacteria by lyophilized nFeS-Hydrogel for improved healing of infected wounds. *Biomater. Adv.* **2022**, *144*, 213207. [CrossRef]

39. Tai, H.; Nishikawa, K.; Higuchi, Y.; Mao, Z.W.; Hirota, S. Cysteine SH and Glutamate COOH Contributions to [NiFe] Hydrogenase Proton Transfer Revealed by Highly Sensitive FTIR Spectroscopy. *Angew. Chem. Int. Ed. Engl.* **2019**, *58*, 13285–13290. [CrossRef]
40. Pandey, P.; Singh, S.P.; Arya, S.K.; Gupta, V.; Datta, M.; Singh, S.; Malhotra, B. Application of thiolated gold nanoparticles for the enhancement of glucose oxidase activity. *Langmuir* **2007**, *23*, 3333–3337. [CrossRef]
41. Sigurdardóttir, S.B.; Lehmann, J.; Ovtar, S.; Grivel, J.C.; Negra, M.D.; Kaiser, A.; Pinelo, M. Enzyme Immobilization on Inorganic Surfaces for Membrane Reactor Applications: Mass Transfer Challenges, Enzyme Leakage and Reuse of Materials. *Adv. Synth. Catal.* **2018**, *360*, 2578–2607. [CrossRef]
42. Fan, R.; Tian, J.; Wang, H.; Wang, X.; Zhou, P. Sensitive colorimetric assay of hydrogen peroxide and glucose in humoral samples based on the enhanced peroxidase-mimetic activity of NH2-MIL-88-derived FeS_2@ CN nanocomposites compared to its precursors. *Microchim. Acta* **2022**, *189*, 1–10. [CrossRef] [PubMed]
43. Shen, B.; Wang, Y.; Wang, X.; Amal, F.E.; Zhu, L.; Jiang, L. A Cruciform Petal-like (ZIF-8) with Bactericidal Activity against Foodborne Gram-Positive Bacteria for Antibacterial Food Packaging. *Int. J. Mol. Sci.* **2022**, *23*, 7510. [CrossRef] [PubMed]
44. Chen, M.; Zhou, H.; Liu, X.; Yuan, T.; Wang, W.; Zhao, C.; Zhao, Y.; Zhou, F.; Wang, X.; Xue, Z.; et al. Single iron site nanozyme for ultrasensitive glucose detection. *Small* **2020**, *16*, 2002343. [CrossRef]
45. Vallabani, N.; Karakoti, A.; Singh, S. ATP-mediated intrinsic peroxidase-like activity of Fe_3O_4-based nanozyme: One step detection of blood glucose at physiological pH. *Colloids Surf. B Biointerfaces* **2017**, *153*, 52–60. [CrossRef]
46. Guo, Y.; Yan, L.; Zhang, R.; Ren, H.; Liu, A. CoO-supported ordered mesoporous carbon nanocomposite based nanozyme with peroxidase-like activity for colorimetric detection of glucose. *Process Biochem.* **2019**, *81*, 92–98. [CrossRef]
47. Lee, G.; Kim, C.; Kim, D.; Hong, C.; Kim, T.; Lee, M.; Lee, K. Multibranched Au–Ag–Pt Nanoparticle as a Nanozyme for the Colorimetric Assay of Hydrogen Peroxide and Glucose. *ACS Omega* **2022**, *7*, 40973–40982. [CrossRef]
48. Kalasin, S.; Sangnuang, P.; Khownarumit, P.; Tang, I.M.; Surareungchai, W. Evidence of Cu(I) Coupling with Creatinine Using Cuprous Nanoparticles Encapsulated with Polyacrylic Acid Gel-Cu(II) in Facilitating the Determination of Advanced Kidney Dysfunctions. *ACS Biomater. Sci. Eng.* **2020**, *6*, 1247–1258. [CrossRef]
49. Robinson, S.; Dhanlaksmi, N. Photonic crystal based biosensor for the detection of glucose concentration in urine. *Photonic Sens.* **2016**, *7*, 11–19. [CrossRef]
50. Chen, W.-H.; Vázquez-González, M.; Zoabi, A.; Abu-Reziq, R.; Willner, I. Biocatalytic cascades driven by enzymes encapsulated in metal–organic framework nanoparticles. *Nat. Catal.* **2018**, *1*, 689–695. [CrossRef]